







Cross-section measurement of the $^{114}\text{Cd}(p, \gamma)^{115m}\text{In}$ reaction for nuclear reactor and astrophysical applications

Vibhuti Vashi ^{1,*}, Rajnikant Makwana ^{1,2,†}, B. Quintana ², M. H. Mehta,³ B. K. Soni,¹ S. Mukherjee,¹ R. K. Singh,¹ R. Chauhan ¹, P. M. Prajapati,⁴ M. Abhangi ³, S. Vala,³ N. L. Singh,¹ G. B. Patel,¹ S. V. Suryanarayana,⁴ B. K. Nayak,⁵ S. C. Sharma,⁶ T. N. Nag,⁷ and Y. Kavun ⁸

¹Physics Department, Faculty of Science, The Maharaja Sayajirao University of Baroda, Vadodra 390002, India

²Departamento de Física Fundamental, Universidad de Salamanca, Calle Espejo s/n, Salamanca 37007, Spain

³Institute for Plasma Research, Gandhinagar, Gujarat 382428, India

⁴Manipal Centre for Natural Sciences, MAHE, Manipal 576014, India

⁵Homi Bhabha National Institute, Anushaktinagar, Mumbai 400094, India

⁶Nuclear Physics Division, Bhabha Atomic Research Centre, Mumbai 400085, India

⁷Radiochemistry Division, Bhabha Atomic Research Centre, Mumbai 400085, India

⁸Department of Medical Imaging Technology, Vocational School of Health Services, Kahramanmaras Sutcu Imam University, Kahramanmaras, Turkey



(Received 1 November 2021; revised 17 December 2021; accepted 11 March 2022; published 18 April 2022)

The present study, carried out for the first time, contributes to the multidisciplinary work in reactor design and nuclear astrophysics. Cadmium has been chosen for the present study for its significant importance in the development of nuclear reactors and for the astrophysical p process. A stacked foil activation technique followed by offline γ -ray spectroscopy were used to carry out the present work. Cross sections were measured for the $^{114}\text{Cd}(p, \gamma)^{115m}\text{In}$ reaction due to the scarcity of data observed in the literature. The S factor was calculated from the cross-section data. The $^{114}\text{Cd}(p, n)^{114m}\text{In}$ reaction was also investigated using the same spectra. Statistical model calculations were performed using the Hauser-Feshbach (HF) code of the latest version of TALYS and were compared with the measured data and the previously measured experimental data available in the literature. A good agreement between theoretical and experimental data was found. The present data follow the trend of theoretical predictions and are in good agreement with the EXFOR database.

DOI: [10.1103/PhysRevC.105.044613](https://doi.org/10.1103/PhysRevC.105.044613)

I. INTRODUCTION

The proton-induced nuclear reactions have significant importance in various fields such as nuclear technology, production of medical radionuclides, radioactive waste management, and nuclear astrophysics [1]. The present work is focused on the field of nuclear reactors and astrophysical applications.

Proton-induced reactions have prime importance in the development of new concepts of nuclear power generation from nuclear reactors. Accelerator-driven subcritical systems (ADSs) [2–5], fast reactors [6,7], compact and high-temperature reactors, and advanced heavy water reactors (AHWRs) [8,9] are the most important candidates. Nuclear data relevant to ADSs, the next-generation reactor, have been a prime interest in recent years. In ADSs, high-energy particles are targeted on a heavy target that produces spallation reactions, which may produce high neutron flux to be used for the transmutation of long-lived isotopes. In addition to the neutrons, other particles such as protons, alpha particles,

and fission fragments will be produced with energy covering the full range up to the GeV range [10,11]. In recent years reactions using these particles became more interesting for finding out suitable materials for the mentioned applications and for withstanding radiation [12].

In fission-based reactors, the fission neutrons slow down in a hydrogenous medium, an appreciable number of fast recoil protons are produced via (n, p) and elastic or inelastic scattering interactions. These protons are capable of initiating nuclear reactions, such as (p, n) and (p, γ) reactions, in light and medium elements [13]. These reactions are of some interest; they can be the origin of various background activities and are used to produce small radioactive sources which cannot be generated in a reactor by other means.

Cadmium is used as a material for control rods in nuclear reactors (AHWRs, pressurized water reactors, etc.) as it has a high cross section to capture low energy neutrons, i.e., thermal neutrons [14]. The recoil protons of the reactor may interact with Cd isotopes and can transmute them into different isotopes, and can change the mechanical and other properties of the controlling material [15]. Cadmium is also used for radiation shielding purposes in nuclear reactors [16]. Moreover, the cross-section data on ^{nat}Cd are also essential for simulating experimental cross-section data measured with

*vibhuti-phyphd@msubaroda.ac.in

†r.j.makwana-phy@msubaroda.ac.in; rajniipr@gmail.com

enriched targets as well for checking the consistency of the evaluated data for different reaction channels [17].

Besides reactor applications, proton-induced reactions have prime importance in the astrophysical p process. The origin of proton-rich stable isotopes with a mass between ^{74}Se and ^{196}Hg , commonly known as “ p nuclei,” has been one of the major open questions [18,19]. In He-accreting sub-Chandrasekhar white dwarfs proton capture reactions are believed to contribute to the production of p nuclei. It is assumed to occur in a zone of core-collapse supernovae, and the peak temperature of the p process lies between $T = 2$ and 3 GK [20]. The p process can also occur in a singly degenerate type-Ia supernova scenario [21]. The vast p process reaction network involves roughly 20 000 reactions among 2000 nuclei from Ni to Bi, which requires attention to the measurement of reaction rates [20]. The $^{114}\text{Cd}(p, \gamma)^{115m}\text{In}$ reaction has significant importance in astrophysics as it is one of the reactions of the “ p process” network. ^{114}Cd is also involved with the p process [22,23].

For the $^{114}\text{Cd}(p, \gamma)^{115m}\text{In}$ reaction, the scarcity of data lies at the higher proton energy range [24,25]. The $^{114}\text{Cd}(p, n)^{114m}\text{In}$ reaction was also studied in the same experiment, and the previously measured data are available in Refs. [26–33]. Our systematic study aims to provide nuclear reaction data where scarcity of data is observed, as nuclear data are a key tool for future reactor development. Additionally, the present data contribute to the existing database of measured cross sections relevant to the astrophysical p process, and help to check the reliability of statistical model calculations over an extensive set of nuclides.

The activation cross sections and astrophysical S factors of $^{114}\text{Cd}(p, \gamma)^{115m}\text{In}$ and $^{114}\text{Cd}(p, n)^{114m}\text{In}$ reactions are presented for the astrophysical and reactor energy ranges in the present study. The astrophysical S factor was measured using cross-section data for both reactions. The latest version of TALYS was used to calculate theoretical cross-section data. The present results are compared with the TALYS data as well as with the available experimental data in the literature compiled in the Exchange Format (EXFOR) database [34]. The present paper contains the following sections: Section II contains the details of the experimental procedure. Section III illustrates the data analysis part which contains the procedures of cross-section measurement and astrophysical S factor determination. Section IV presents the overview of theoretical calculations, followed by results and discussions in Sec. V. A summary and conclusions are given in Sec. VI.

II. EXPERIMENTAL DETAILS

The experiment was performed using the stacked foil activation technique followed by offline γ -ray spectroscopy at the BARC-TIFR Pelletron facility [35], Mumbai, India. In the present experiment, $^{\text{nat}}\text{Cd}$ of ≈ 250 micron thickness was used as a target, and copper (Cu) foil of ≈ 3.56 micron thickness was used as an energy degrader in between the target layers to reduce the significant proton beam energy. A constant current of 150 nA was used for the proton beam during the experiment. The degradation of proton energy by each target was calculated using MCNP 6.2 code [36] and is shown in Fig. 1.

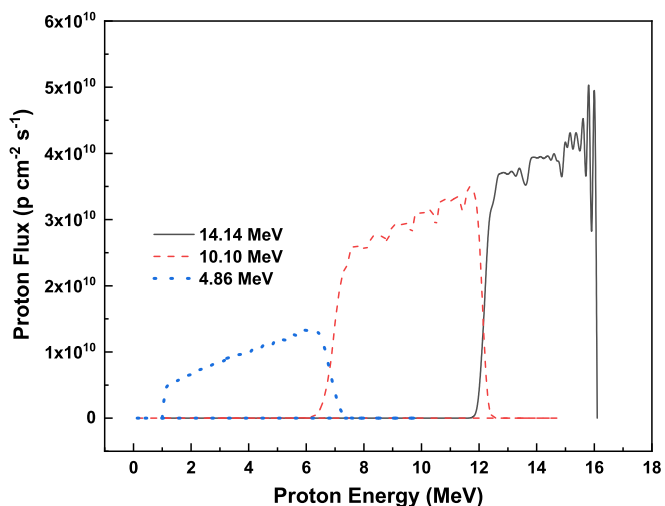


FIG. 1. Proton energy degradation using MCNP 6.2 code.

A schematic diagram of the experimental arrangement is presented in Fig. 2. The aluminum-foil-wrapped stack was placed inside the 6 m irradiation port, just before the analyzing magnets in the main beam line of the pelletron. A proper circular-shaped proton beam was obtained when the beam was made to pass through the 6 mm aperture of a tantalum collimator. The stack was irradiated for sufficient time to build an ample amount of activity. The irradiated samples were allowed to cool down for sufficient time to reduce the radiation dose. Then, the samples were taken for γ -ray counting to a precalibrated 80 cm^3 high-purity germanium (HPGe) detector connected to PC based 4096 channel analyzer. The HPGe detector was calibrated using a ^{152}Eu multi- γ -ray source. The characteristic γ lines with their respective half-lives were used to identify the residual nuclei of interest. All the spectroscopic data used in the present calculations were taken from the NuDat [37] database, whereas the Q values and the threshold energies were taken from QTOOL [38], as indicated in Table I.

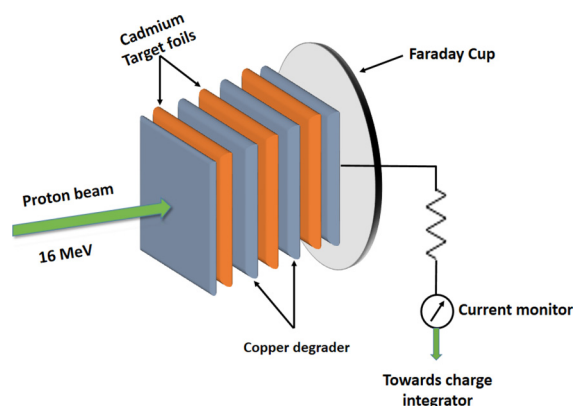


FIG. 2. A schematic diagram of the stacked foil experiment [40,41].

TABLE I. Isotopic abundance of targets, threshold energy of reaction, product nucleus half-life, and energies of prominent γ -rays with branching intensities of selected nuclear reactions.

Reaction	Isotopic abundance [39] (%)	Threshold energy [38] (MeV)	Half-life [37]	Prominent γ -ray energy [37] (keV)	Branching intensity [37] (%)
$^{114}\text{Cd}(p, \gamma)^{115m}\text{In}$	28.73	0.0	4.486(4) h	336.24(25)	45.9(1)
$^{116}\text{Cd}(p, 2n)^{115m}\text{In}$	7.49	8.099	4.486(4) h	336.24(25)	45.9(1)
$^{114}\text{Cd}(p, n)^{114m}\text{In}$	28.73	2.247	49.51(1) d	190.27(3)	15.56(15)
$^{113}\text{Cd}(p, \gamma)^{114m}\text{In}$	12.22	0.0	49.51(1) d	190.27(3)	15.56(15)

III. DATA ANALYSIS

A. Cross-section measurement

The activation cross sections of $^{114}\text{Cd}(p, \gamma)^{115m}\text{In}$ [$Q = 6810.4(0.3)$ keV] and $^{114}\text{Cd}(p, n)^{114m}\text{In}$ [$Q = -2227.5(0.4)$ keV] reactions were measured for three proton energies, 14.26 ± 2.03 , 10.18 ± 2.15 , and 4.90 ± 2.40 MeV in the laboratory frame.

The activation analysis technique is used for the measurement of reaction cross sections by irradiating target nuclei with a proton beam. The products that emerge as a result of irradiation must have a sufficiently long half-life and γ -branching abundances. The cross sections of chosen reactions were measured using the activation formula [42,43]

$$\sigma_R = \frac{A_\gamma \lambda \left(\frac{t_c}{t_r}\right) e^{\lambda t_w}}{N \epsilon I_\gamma \phi (1 - e^{-\lambda t_i})(1 - e^{-\lambda t_c})}, \quad (1)$$

where σ_R is the reaction cross section; A_γ the number of detected γ rays; λ the decay constant of product nuclei (s^{-1}); t_c the counting time (s); t_r the real time (s); t_w the cooling time (s); N the number of target atoms; ϕ the proton flux incident on the target ($\text{p cm}^{-2}\text{s}^{-1}$); I_γ the branching intensity of γ rays; and ϵ the efficiency of the detector for the desired γ ray.

In the above equation, activity A_γ is measured from the γ -ray spectra obtained using the HPGe detector. The number of targets was calculated using the weight of the sample and isotopic abundance. The details of emitted prominent γ rays and half-lives of daughter nuclei are taken from the literature [44]. A typically recorded γ -ray spectrum for the irradiated cadmium sample at ≈ 16 MeV proton energy is shown in Fig. 3.

As cadmium has eight isotopes, various reaction channels may produce the same radionuclide as a reaction product. For the present case, the ^{115m}In radionuclide is produced as a reaction product from $^{114}\text{Cd}(p, \gamma)^{115m}\text{In}$ and $^{116}\text{Cd}(p, 2n)^{115m}\text{In}$ reaction channels. As the threshold energy of $(p, 2n)$ reaction is 8.099 MeV, this particular channel opens up after this threshold and it will contribute to 14.26 ± 2.03 and 10.18 ± 2.14 MeV proton energies for the $^{114}\text{Cd}(p, \gamma)^{115m}\text{In}$ reaction. Thus, the activity of a photopeak for the 336.24 keV γ ray from ^{115m}In has been delineated using a technique explained in the literature [45,46]. A factor, i.e., the activity ratio, of the 336.24 keV γ ray of ^{115m}In from $^{114}\text{Cd}(p, \gamma)^{115m}\text{In}$ and $^{116}\text{Cd}(p, 2n)^{115m}\text{In}$ reactions was calculated using the following equation:

$$\text{Factor} = A_{\text{obs}} \text{ from } (p, \gamma) \text{ reaction} / A_{\text{obs}} \text{ from } (p, 2n) \text{ reaction}$$

$$\begin{aligned} &= \frac{N \sigma_{(p, \gamma)} \phi \epsilon (1 - e^{-\lambda t_i})(1 - e^{-\lambda t_c}) e^{\lambda t_w} / \lambda}{N \sigma_{(p, 2n)} \phi \epsilon (1 - e^{-\lambda t_i})(1 - e^{-\lambda t_c}) e^{\lambda t_w} / \lambda} \\ &= \frac{a_{114} \sigma_{(p, \gamma)}}{a_{116} \sigma_{(p, 2n)}}, \end{aligned} \quad (2)$$

where a_{114} and a_{116} are the isotopic abundances of ^{114}Cd and ^{116}Cd , respectively. $\sigma_{(p, \gamma)}$ and $\sigma_{(p, 2n)}$ are the reaction cross sections calculated using the nuclear modular code TALYS-1.95 [47] for both reactions. A brief description of the TALYS calculation is presented in the next section. The activity of the individual reaction product was obtained using the activity ratio (factor) and total activity of the 336.24 keV γ ray of ^{115m}In from $^{114}\text{Cd}(p, \gamma)^{115m}\text{In}$ and $^{116}\text{Cd}(p, 2n)^{115m}\text{In}$ reactions. Once the photopeak activity of the 336.24 keV γ -ray energy of ^{115m}In from the above mentioned reactions was delineated, the individual reaction cross sections were calculated using Eq. (2).

The technique explained above was also used for the $^{114}\text{Cd}(p, n)^{114m}\text{In}$ reaction as ^{114m}In is the product nucleus produced from $^{114}\text{Cd}(p, n)^{114m}\text{In}$ and $^{113}\text{Cd}(p, \gamma)^{114m}\text{In}$ reaction channels.

B. The standard approximation of the Gamow window and S factor determination

The nuclear reactions in stars will occur near the energies where the product of velocity distribution and the cross

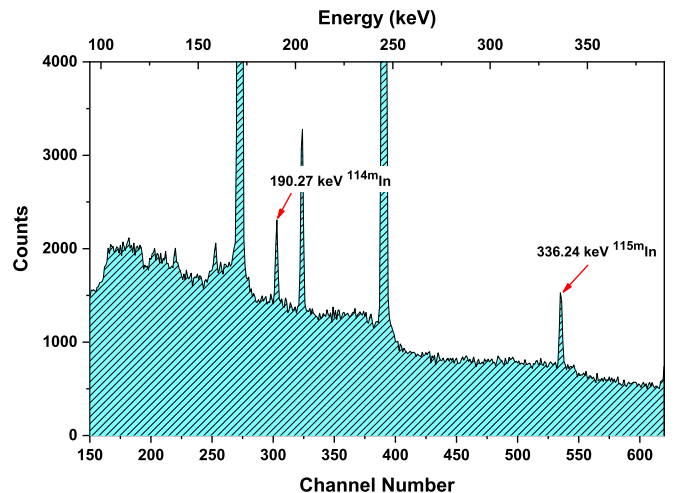


FIG. 3. A typical γ -ray energy spectrum obtained from the interaction of $p+^{114}\text{Cd}$ at $E_p \approx 16$ MeV.

section is at maximum. The standard approximation of the Gamow window assumes that the energy dependence of the cross section σ is mainly determined by the projectile's penetration of the Coulomb barrier (the Gamow factor $e^{-2\pi\eta}$) and a part representing the weakly energy-dependent properties of the nuclear interior (the astrophysical S factor). The nonresonant reaction rate is given by [48,49]

$$\langle\sigma v\rangle = \left(\frac{8}{\pi\mu}\right)^{\frac{1}{2}} \frac{1}{(kT)^{\frac{3}{2}}} \int_0^{\infty} S(E)e^{-E/kT} e^{-2\pi\eta} dE, \quad (3)$$

where $S(E)$ is the astrophysical S factor defined by [50]

$$S(E) = \frac{\sigma(E)E}{e^{-2\pi\eta}}, \quad (4)$$

which is assumed to be only weakly dependent on the energy E for nonresonant reactions. The astrophysical S factor is a rescaled variant of the nuclear reaction's total cross section $\sigma(E)$ which is required for many astrophysical applications specifically for energies below the Coulomb barrier. The S factor varies much more smoothly with the energy compared to the cross section, thus allowing for safer extrapolations to the experimentally inaccessible energy range [23,51].

The second exponential in Eq. (3) contains an approximation of the Coulomb penetration through the Sommerfeld parameter η ,

$$\eta = \frac{Z_1 Z_2 e^2}{\hbar} \sqrt{\frac{\mu}{2E}}, \quad (5)$$

where Z_1 and Z_2 describe the charges of projectile and target, respectively, and μ is the reduced mass. In Eq. (3), while the first exponential decreases with increasing energy, this second one increases, leading to a confined peak of the integrand, the so-called Gamow peak. The location of the peak is shifted to higher energies with respect to the maximum of the Maxwell-Boltzmann distribution at $E_{MB} = kT$.

The exponent can be approximated in numerical units by

$$2\pi\eta = 31.29Z_1Z_2\sqrt{\frac{\mu}{E_{\text{c.m.}}}}, \quad (6)$$

where the center-of-mass energy $E_{\text{c.m.}}$ is in keV and the reduced mass μ is in amu (atomic mass units).

For a given stellar environment, the charged-particle-induced nuclear reactions take place in this relatively narrow energy window around the E_0 effective burning energy. This can be obtained by the first derivative of the integrand yields [52–54]

$$E_0 = \left(\frac{\mu}{2}\right)^{\frac{1}{3}} (kT)^{\frac{2}{3}}, \quad (7)$$

$$E_0 = 0.12204(\mu Z_1^2 Z_2^2 T_9^2)^{\frac{1}{3}}.$$

The effective width Δ of the energy window can be defined as

$$\Delta = 0.23682(\mu Z_1^2 Z_2^2 T_9^5)^{\frac{1}{6}}. \quad (8)$$

Here E_0 and Δ are in units of MeV and T_9 is the plasma temperature in GK, Equations (7) and (8) are widely used to

determine a relevant energy range $E_0 - (\Delta/2) \leq E \leq E_0 + (\Delta/2)$ within which the nuclear cross sections have to be known. This region represents the effective energy window for nonresonant thermonuclear reactions in stars [49]. This window shifts towards higher energy and becomes broader for increasing temperature according to Eqs. (7) and (8). These equations are important to design experiments and are valid for sufficiently low temperature and constant astrophysical S factor.

In the present study, the proton energy of 4.90 ± 2.40 MeV lies in the range of the Gamow window for the temperatures related to the production of p nuclei at $T_{\text{peak}} = 5$ GK. Moreover, the astrophysical S factor has been measured for both reactions. The $^{114}\text{Cd}(p, n)^{114m}\text{In}$ reaction has limited utility as the reaction has negative Q value [$Q = -2227.5(0.4)$ keV].

IV. THEORETICAL CALCULATION

TALYS-1.95, a computer code is utilized to perform the theoretical calculation using the Hauser-Feshbach (HF) statistical model [47,55]. The reaction parameters are chosen from the IAEA Reference Input Parameter Library (RIPL) database [56]. TALYS consists of different nuclear models for direct, compound, preequilibrium, and fission reaction mechanisms as a function of incident particle energy. The code uses optical model parameters which were acquired using local and global potentials proposed by Koning and Delaroche [57]. The Hauser-Feshbach model is accounted for by studying compound reaction mechanisms [58]. The precompound (preequilibrium) reactions were solved using the exciton model proposed by Kalbach [59].

We used a total of 96 different combinations of the main ingredients of the model, i.e., the optical model potential (OMP) (two default options), the nuclear level density (NLD) (six default options), and the γ -ray strength function (γ -SF) (eight default options). For the OMP, we used the phenomenological model of Koning-Delaroche [57] and the semimicroscopic model of Bauge-Delaroche-Girod [60]. Six nuclear level density (NLD) models are available in TALYS code: the phenomenological constant temperature model (CTM)[61], the back-shifted Fermi gas model (BSFG) [62], the generalized superfluid model (GSM) [63], the semimicroscopic level density tables of Goriely (HFBC) [64] and Goriely *et al.* (HFB) [65], and the time-dependent Hartree-Fock-Bogolyubov method combined with the Gogny force (HFB-T) [66]. We also employed γ -ray strength functions such as Kopecky-Uhl (KU) [67] and the Brink-Axel (BA) generalized Lorentzians [68,69], the Hartree-Fock-BCS (HFBCS/QRPA) and Hartree-Fock-Bogolyubov methods (HFB/QRPA), Goriely's hybrid model (HG) [70], as well as Goriely's tables using the temperature-dependent Hartree-Fock-Bogolyubov method. Lastly, we employed models using the temperature-dependent relativistic mean-field method [66] and the Hartree-Fock-Bogolyubov method along with the quasiparticle-random-phase approximation (QRPA) using the Gogny D1M interaction [71].

After performing all the calculations with the models noted above, the maximum and minimum for each energy were defined with the borders of the light blue area as shown in

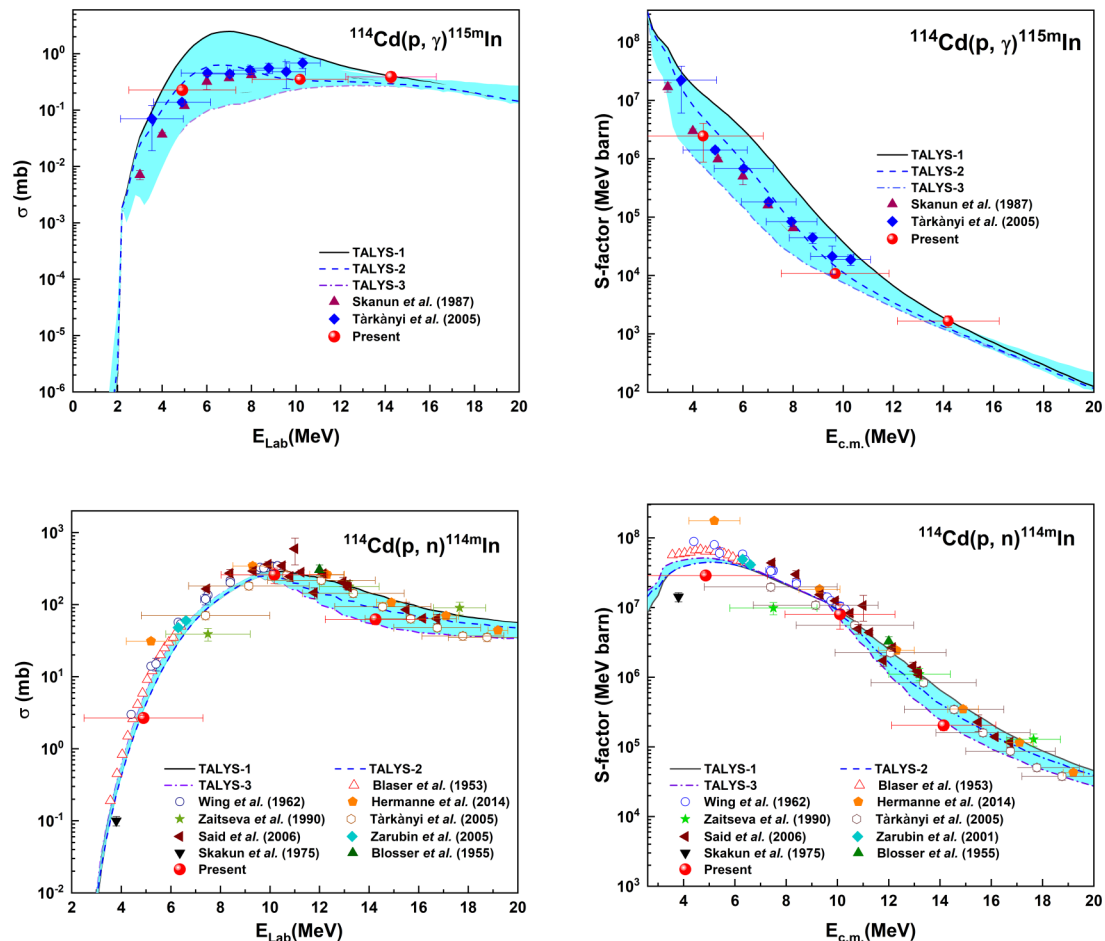


FIG. 4. Upper panel: Comparison of the cross sections for the $^{114}\text{Cd}(p, \gamma)^{115m}\text{In}$ reaction with three different HF calculations using the TALYS-1, TALYS-2, and TALYS-3 combinations (see Sec. IV for details) and with the data retrieved from the literature (Skakun 1987 [24], Tarkanyi 2005 [25]). Lower panel: Comparison of the cross-section data for the $^{114}\text{Cd}(p, n)^{114m}\text{In}$ reaction with three different HF calculations using the TALYS-1, TALYS-2, and TALYS-3 combinations (see Sec. IV for details) and with the data retrieved from the literature (Blaser 1953 [26], Wing 1962 [27], Hermanne 2014 [28], Zaitseva 1990 [29], Tarkanyi 2005 [25], Said 2006 [30], Zarubin 2001 [31], Skakun 1975 [32], Blosser 1955 [33]). The corresponding astrophysical S factors are plotted in the right panel.

Fig. 4. The best fit isomer calculation is directly compared with the experimental data and EXFOR database. The graph shows different combinations of TALYS code as follows: For the $^{114}\text{Cd}(p, \gamma)^{115m}\text{In}$ reaction, TALYS-1 and TALYS-2 employ the Bauge-Delaroche-Girod OMP [using the approach of Jeukenne, Lejeune, and Mahaux (JLM)] and the Brink-Axel (BA) Lorentzian γ -SF model, whereas TALYS-3 employs the Koning-Delaroche (KD) OMP and Kopecky-Uhl (KU) generalized Lorentzian γ -SF model; TALYS-2 and TALYS-3 employ the generalized superfluid model (GSM) NLD, whereas TALYS-1 employs the back-shifted Fermi gas model (BSM) NLD.

For the $^{114}\text{Cd}(p, n)^{114m}\text{In}$ reaction, TALYS-1 and TALYS-2 employ the Bauge-Delaroche-Girod (JLM) OMP and TALYS-3 employs the Koning-Delaroche (KD) OMP. TALYS-1 employs microscopic level densities (Skyrme force) from Hilaire's combinatorial tables (HFB) of the NLD and Kopecky-Uhl (KU) generalized Lorentzian γ -SF model. TALYS-2 employs microscopic level densities (Skyrme force) from Goriely's tables (HFBCS) and Hartree-Fock-Bogolyubov

tables (HFB/QRPA) of the γ -SF model whereas TALYS-3 employs the generalized superfluid (GSM) NLD and T -dependent relativistic mean field (RMF) γ -SF model.

V. RESULTS AND DISCUSSION

The cross sections were measured for $^{114}\text{Cd}(p, \gamma)^{115m}\text{In}$ reaction in the energy range where the data are scarce. The cross sections were also measured for $^{114}\text{Cd}(p, n)^{114m}\text{In}$ reaction using the same γ -ray spectra. The cross-section data were measured for different proton energies of 14.26 ± 2.03 , 10.18 ± 2.15 , and 4.90 ± 2.40 MeV for both reactions, which have eminent importance for reactor applications, and the lowest energy lies in the Gamow window of the astrophysical energy range. The error in proton energy represents the thickness of the cadmium target. The comparison of theoretical calculations of TALYS-1.95 with our measured experimental data obtained in the present work is shown in Fig. 4 along with the available experimental data from the EXFOR database [34]. The range of uncertainties of the measured cross

TABLE II. Cross sections and astrophysical S factors for the $^{114}\text{Cd}(p, \gamma)^{115m}\text{In}$ and $^{114}\text{Cd}(p, n)^{114m}\text{In}$ reactions.

E_p (MeV)	$E_{c.m.}$ (MeV)	E_{lab} (MeV)	$^{114}\text{Cd}(p, \gamma)^{115m}\text{In}$		$^{114}\text{Cd}(p, n)^{114m}\text{In}$	
			Cross section (mb)	S factor (10^6 MeV b)	Cross section (mb)	S factor (10^6 MeV b)
16.00	14.14	14.26 ± 2.03	0.389 ± 0.087	0.0017	47.60 ± 7.53	0.2037
12.27	10.10	10.18 ± 2.15	0.351 ± 0.044	0.0108	258.72 ± 63.31	7.9908
7.83	4.86	4.90 ± 2.40	0.227 ± 0.054	2.4542	2.67 ± 0.23	28.8429

sections is shown by the shaded areas. The upper and lower borders of the shaded region correspond to the highest and lowest cross-section values of TALYS-1.95, respectively. The results were not obtained from a single combination of TALYS input.

For the $^{114}\text{Cd}(p, \gamma)^{115m}\text{In}$ reaction, the upper border of the shaded region is the combination of JLM OMP with BSM NLD and BA γ -SF named TALYS-1. The lower border of the shaded region is the combination of KD OMP with GSM NLD and KU γ -SF named TALYS-3. The data points of 14.26 ± 2.03 and 10.18 ± 2.15 MeV lie close to the results of TALYS-2 and TALYS-3. The cross-section value of 4.90 ± 2.40 MeV is well matched with the results of TALYS-2, which is the combination of JLM OMP, GSM NLD and BA γ -SF. The presently measured data are well inside the region and follow the trend of previously available data from the EXFOR database and the predicted data of nuclear model code TALYS. The data point measured at 14.26 ± 2.03 MeV can help us to understand the trend.

For the $^{114}\text{Cd}(p, n)^{114m}\text{In}$ reaction, the upper border of the shaded region is the combination of JLM OMP with HFB NLD and KU γ -SF named TALYS-1. The lower border of the shaded region is the combination of KD OMP with GSM NLD and T -dependent RMF γ -SF named TALYS-3. The present measurements are in the range of predicted data of TALYS. The data points of 14.26 ± 2.03 and 4.90 ± 2.40 MeV are slightly suppressed compared to the existing data points and combinations of TALYS. The cross-section value of 10.18 ± 2.15 MeV is in good agreement with all combinations of TALYS and the literature data. The cross-section value of 4.90 ± 2.40 MeV is well matched with the results of TALYS-3. Overall the experimental data follow the trend of TALYS-1.95 and are in good agreement with literature data for both reactions.

The astrophysical S factor was also determined using cross-section data for both reactions and is shown in the right panel of Fig. 4. It shows the comparison of presently measured S factor data with the theoretical prediction of TALYS-1.95 and available data of the EXFOR database. The measured

data follow the trend of theoretical predictions of TALYS-1.95 and are in good agreement with the EXFOR database. The measured spectrum average cross sections and astrophysical S factors for both the reactions are given in Table II.

VI. SUMMARY AND CONCLUSION

In the framework of the present paper, multidisciplinary work is carried out in the field of nuclear reactors and astrophysics. The present work will enhance the nuclear data library of proton-induced nuclear reactions for reactor applications. Also, the present work is a small contribution to the astrophysical p process. The experiment on the proton-induced reaction on cadmium was carried out using the stacked foil activation analysis technique followed by offline γ -ray spectroscopy. The cross sections were measured for $^{114}\text{Cd}(p, \gamma)^{115m}\text{In}$ and $^{114}\text{Cd}(p, n)^{114m}\text{In}$ reactions for three different proton energies, 14.26 ± 2.03 , 10.18 ± 2.15 , and 4.90 ± 2.40 MeV in the laboratory frame. The astrophysical S factor was also determined for all three energies in the center-of-mass frame. The presently measured data are in good agreement with available experimental data of the EXFOR database and with the data obtained from nuclear model code TALYS-1.95 for both reactions. Both experimental and theoretical studies are required to gain firm insight into the driving mechanisms behind the p process nucleosynthesis and restrict the parameters of the theoretical models in an energy region where a scarcity of experimental data, even for stable nuclei, still persists.

ACKNOWLEDGMENTS

R.J.M. acknowledges the UGC-DAE Consortium for Scientific Research, Kolkata Centre for providing the project grant UGC.DAE-CSR-KC/CRS/19NPO8/0919 to carry out research work. The authors are also thankful to the BARC-TIFR Pelletron staff for providing the beam and allowing us to use the facility.

[1] F. Tarkanyi *et al.*, *Nucl. Instrum. Methods Phys. Res., Sect. B* **245**, 379 (2006).

[2] F. Carminati, R. Klapisch, J. P. Revol, Ch. Roche, J. A. Rubio, and C. Rubbia, An Energy Amplifier for Cleaner and Inexhaustible Nuclear Energy Production Driven by Particle Beam

Accelerator, CERN Report No. CERN/AT/93-47 (ET), 1993 (unpublished).

[3] C. Rubbia, J. A. Rubio, S. Buono, F. Carminati, N. Fietier, J. Galvez, C. Geles, Y. Kadi, R. Klapisch, P. Mandrilion, J. P. Revol, and Ch. Roche, Conceptual Design of a Fast Neutron

- Operated High Power Energy Amplifier, CERN Report No. CERN/AT/95-44 (ET), 1995 (unpublished).
- [4] *The International Conference on Accelerator-Driven Transmutation Technologies and Applications, Las Vegas, Nevada, 1994*, edited by E. D. Arthur, S. A. Schriber, and A. Rodriguez, AIP Conf. Proc. No. 346 (AIP, New York, 1995).
- [5] Muhammad Shahid *et al.*, *Nucl. Instrum. Methods Phys. Res., Sect. B* **342**, 305 (2015).
- [6] R. K. Sinha and A. Kakodkar, *Nucl. Eng. Des.* **236**, 683 (2006).
- [7] S. Ganesan, Creation of Indian Experimental Benchmarks for Thorium Fuel Cycle, IAEA Coordinated Research Project on Evaluated Data for Thorium-Uranium fuel Cycle, Third Research Co-ordination Meeting, 30 January to 2 February 2006, Vienna, Austria, IAEA Report No. INDC(NDS)-0494, 2006 (unpublished).
- [8] L. Mathieu *et al.*, Proposal for a simplified thorium molten salt reactor, in *Proceedings of the GLOBAL International Conference* (Tsukuba, Japan, 2005), p. 428.
- [9] International Atomic Energy Agency, Thorium Fuel Utilization: Options and Trends, IAEA Report No. IAEA-TECDOC-1319, Nov. 2002 (unpublished).
- [10] F.-R. Lecolley *et al.*, in *International Conference on Nuclear Data for Science and Technology, 26 September – 1 October 2004, Santa Fe*, edited by R. C. Haight, M. B. Chadwick, T. Kawano, and P. Talou, AIP Conf. Proc. No. 769 (AIP, New York, 2005), p. 61.
- [11] G. R. Grant and L. Yaffe, *Can. J. Chem.* **41**, 2533 (1963).
- [12] T. Allen *et al.*, *Mater. Today* **13**, 14 (2010).
- [13] S. S. Glickstein and R. G. Winter, *Nucl. Instrum. Methods* **9**, 226 (1960).
- [14] D. A. Petti, *Nucl. Technol.* **84**, 128 (1989).
- [15] S. T. Mongelli *et al.*, *Braz. J. Phys.* **35**, 894 (2005).
- [16] Y. S. Alajerami *et al.*, *J. Appl. Phys.* **127**, 175102 (2020).
- [17] F. S. Al-Saleh, *Radiochim. Acta* **96**, 461 (2008).
- [18] E. M. Burbidge, G. R. Burbidge, W. A. Fowler, and F. Hoyle, *Rev. Mod. Phys.* **29**, 547 (1957).
- [19] A. G. W. Cameron, *Publ. Astron. Soc. Pac.* **69**, 201 (1957).
- [20] M. Arnould and S. Goriely, *Phys. Rep.* **384**, 1 (2003).
- [21] C. Travaglio, F. K. Röpke, R. Gallino, and W. Hillebrandt, *Astrophys. J.* **739**, 93 (2011).
- [22] K. Wisshak, F. Voss, F. Käppeler, and L. Kazakov, *Phys. Rev. C* **66**, 025801 (2002).
- [23] A. Psaltis, A. Khaliel, E.-M. Assimakopoulou, A. Kanellakopoulos, V. Lagaki, M. Lykiardopoulou, E. Malami, P. Tsavalas, A. Zyriliou, and T. J. Mertzimekis, *Phys. Rev. C* **99**, 065807 (2019).
- [24] E. A. Skakun *et al.*, *Yad. Fiz.* **45**, 614 (1987).
- [25] F. Tärkányi *et al.*, *Radiochim. Acta* **93**, 561 (2005).
- [26] J. -P. Blaser, F. Boehm, P. Marmier, and D. C. Peaslee, *Helv. Phys. Acta* **24**, 3 (1951).
- [27] J. Wing and J. R. Huizenga, *Phys. Rev.* **128**, 280 (1962).
- [28] A. Hermanne *et al.*, *Radiochimica Acta* **102**, 1111 (2014).
- [29] N. G. Zaitseva *et al.*, *Appl. Radiat. Isot.* **41**, 177 (1990).
- [30] S. A. Said, E. K. Elmaghraby, and F. I. Asfour, *Appl. Radiat. Isot.* **64**, 1655 (2006).
- [31] P. P. Zarubin and V. O. Sergeev, *Russ. Akad. Nauk, Ser. Fiz.* **65**, 1612 (2001).
- [32] E. A. Skakun, A. P. Klyucharev, Y. N. Rakivnenko, and I. A. Romani, *Izvestiya Ross. Akad. Nauk, Ser. Fiz.* **39**, 24 (1975).
- [33] H. G. Blosser and T. H. Handley, *Phys. Rev.* **100**, 1340 (1955).
- [34] Cross-Section Information Storage and Retrieval System (EXFOR), IAEA, Vienna, <http://www.nds.iaea.or.at/exfor/>
- [35] BARC-TIFR Pelletron facility, Mumbai, official website: <https://www.tifr.res.in/~pell/pelletron/index.php>
- [36] MCNP Users Manual - Code Version 6.2, edited by C. J. Werner, Los Alamos National Laboratory Report No. LA-UR-17-29981, 2017 (unpublished).
- [37] NuDat 2.7 β 2011, National Nuclear Data Center, Brookhaven National Laboratory, official website: <https://www.nndc.bnl.gov/nudat2/>
- [38] Qtool: calculation of reaction Q-values and threshold, Los Alamos National Library, official website: http://cdfc.sinp.msu.ru/services/calc_thr/calc_thr.html
- [39] K. J. R. Rosman and P. D. P. Taylor, *Pure Appl. Chem.* **70**, 217 (1998).
- [40] S. Parashari, S. Mukherjee, S. V. Suryanarayana, R. Makwana, B. K. Nayak, A. Shanbhag, and H. Naik, *Nucl. Phys. A* **979**, 102 (2018).
- [41] S. Parashari, S. Mukherjee, B. K. Nayak, R. Makwana, S. V. Suryanarayana, H. Naik, and S. C. Sharma, *Nucl. Phys. A* **978**, 160 (2018).
- [42] R. Makwana, S. Mukherjee, P. Mishra, H. Naik, N. L. Singh, M. Mehta, K. Katovsky, S. V. Suryanarayana, V. Vansola, Y. Santhi Sheela, M. Karkera, R. Acharya, and S. Khirwadkar, *Phys. Rev. C* **96**, 024608 (2017).
- [43] V. Vashi, R. Makwana, S. Mukherjee, B. K. Soni, M. H. Mehta, S. Parashari, R. K. Singh, R. Chauhan, S. V. Suryanarayana, B. K. Nayak, S. C. Sharma, H. Naik, N. L. Singh, and T. N. Nag, *Eur. Phys. J. Plus* **136**, 746 (2021).
- [44] http://www.nndc.bnl.gov/nudat2/indx_dec.jsp, retrieved on 21 March 2020.
- [45] D. L. Smith, J. W. Meadows, P. A. Moldauer, and W. P. Poenitz, *Nucl. Phys. A* **388**, 37 (1982).
- [46] Reetuparna Ghosh *et al.*, *J. Radioanal. Nucl. Chem.* **307**, 1481 (2016).
- [47] A. Koning, S. Hilaire, and S. Goriely, *TALYS-1.95 - A Nuclear Reaction Program, User Manual*, 1st ed. (NRG, Petten, 2017).
- [48] T. Rauscher, F.-K. Thielemann, and K.-L. Kratz, *Phys. Rev. C* **56**, 1613 (1997).
- [49] J. R. Newton, C. Iliadis, A. E. Champagne, A. Coc, Y. Pappas, and C. Ugalde, *Phys. Rev. C* **75**, 045801 (2007).
- [50] C. Yalcin, R. T. Güray, N. Ozkan, S. Kutlu, Gy. Gyürky, J. Farkas, G. G. Kiss, Zs. Fülöp, A. Simon, E. Somorjai, and T. Rauscher, *Phys. Rev. C* **79**, 065801 (2009).
- [51] V. Singh, J. Lahiri, and D. N. Basu, *Nucl. Phys. A* **987**, 260 (2019).
- [52] C. E. Rolfs and W. S. Rodney, *Cauldrons in the Cosmos* (University of Chicago Press, Chicago, 1988).
- [53] W. A. Fowler, G. E. Caughlan, and B. A. Zimmerman, *Annu. Rev. Astron. Astrophys.* **5**, 525 (1967).
- [54] T. Rauscher, *Phys. Rev. C* **81**, 045807 (2010).
- [55] A. J. Koning, S. Hilaire, and M. C. Duijvestijn, in *ND2007, International Conference on Nuclear Data for Science and Technology* (EDP Sciences, Les Ulis, France, 2007), pp. 211–214.
- [56] R. Capote *et al.*, *Nucl. Data Sheets* **110**, 3107 (2009).
- [57] A. J. Koning and J. P. Declaroche, *Nucl. Phys. A* **713**, 231 (2003).
- [58] W. Hauser and H. Feshbach, *Phys. Rev.* **87**, 366 (1952).
- [59] C. Kalbach, *Phys. Rev. C* **33**, 818 (1986).

- [60] E. Bauge, J. P. Delaroche, and M. Girod, *Phys. Rev. C* **63**, 024607 (2001).
- [61] A. Gilbert and A. G. W. Cameron, *Can. J. Phys.* **43**, 1446 (1965).
- [62] W. Dilg, W. Schantl, H. Vonach, and M. Uhl, *Nucl. Phys. A* **217**, 269 (1973).
- [63] A. V. Ignatyuk, J. L. Weil, S. Raman, and S. Kahane, *Phys. Rev. C* **47**, 1504 (1993).
- [64] S. Goriely, F. Tondeur, and J. M. Pearson, *At. Data Nucl. Data Tables* **77**, 311 (2001).
- [65] S. Goriely, S. Hilaire, and A. J. Koning, *Phys. Rev. C* **78**, 064307 (2008).
- [66] S. Hilaire, M. Girod, S. Goriely, and A. J. Koning, *Phys. Rev. C* **86**, 064317 (2012).
- [67] J. Kopecky and M. Uhl, *Phys. Rev. C* **41**, 1941 (1990).
- [68] D. M. Brink, *Nucl. Phys.* **4**, 215 (1957).
- [69] P. Axel, *Phys. Rev.* **126**, 671 (1962).
- [70] S. Goriely, *Phys. Lett. B* **436**, 10 (1998).
- [71] M. Martini, S. Hilaire, S. Goriely, A. Koning, and S. Pru, *Nucl. Data Sheets* **118**, 273 (2014).